Batteries & Supercaps

Research Article
doi.org/10.1002/batt.202200430

Chemistry Europe
European Chemical Societies Publishing

www.batteries-supercaps.org

Revisiting the Relation Between the Stability of the LUMO of the Electrolytes and the Kinetics of Solid Electrolyte Interface Formation in Lithium- and Post-Lithium-ion Batteries

Mithun C. Madhusudhanan,[a] Sreelakshmi Anil Kumar,[b] Swetha Nair,[a] Nikitha Srinivasan,[c] Madhurja Buragohain,[c] and Sooraj Kunnikuruvan*[c]

Despite their high theoretical capacity, the practical application of Li-ion batteries (LIBs) and post-LIBs with metal anodes are limited due to their poor safety and electrochemical performance. Solid electrolyte interface (SEI) was found to have an important role in this. It was found that SEI on metal anodes is overgrown and non-uniform owing to their high reactivity, which in turn affects the performance of metal anode-based batteries. Recent studies indicate that modulating the properties of the SEI is a good strategy to improve the electrochemical performance of batteries. In this regard, identifying the critical reactivity descriptors that can provide insights into the SEI formation kinetics is of large importance. Herein, we performed computational studies involving 53 selected ion-solvent complexes that represent 53 commonly used electrolytes and 12 salt molecules in LIBs and post-LIBs. Unlike previous studies which considered the LUMO energy of the electrolyte as the suitable chemical reactivity descriptor, this study shows that electron affinity and electrophilicity of the individual ions and solvents that constitute the electrolytes are more suitable and general chemical reactivity descriptors for predicting the SEI formation kinetics. In addition to suggesting suitable approaches to modulate the SEI formation kinetics, this study also brings light to the critical role of the ion-solvent combination in determining the SEI formation kinetics.

Introduction

The development of metal anode-based Lithium and post-Li ion batteries is the most sought-after for high energy density batteries owing to their high theoretical capacities.[1–4] In spite of their huge potential, metal anode-based batteries are suffering from poor safety and electrochemical performance in practice.[5–7] This can be ascribed to the high reactivity of the metal surfaces and related dendrite formation.[8,9] Moreover, identifying stable cathode and electrolytes is also found to be challenging.[5–7]

One of the important factors that affect the electrochemical performance of the batteries is the electrode-electrolyte interface (EEI). The EEI on anodes is popularly known as the solid-electrolyte interface (SEI) and is formed by the reductive decomposition of electrolytes on the anode surface. An ideal SEI is a stable passivating layer that allows the passage of ions and prevents the conduction of electrons.[10–13] Thus SEI acts as a protecting layer and prevents further decomposition of the electrolyte.[7,13–18] However, an overgrown or non-uniform SEI that can be formed on highly reactive metal anode surfaces could result in poor cycling stability and capacity fading. Therefore, a stable SEI with optimal thickness is crucial for the good electrochemical performance of metal anode-based batteries. In this regard, an appropriate choice of electrodes and electrolytes that can result in stable SEI is vital for the development of high-energy density and stable metal anode-based batteries. The development of high-performance batteries by tuning the properties of EEI has thus gained a lot of attention and is an active area of research.[19–21]

A thorough understanding of the mechanism of formation and the structure of SEI as well as the electronic structure of the surface and the electrolytes are vital for designing and modulating the properties of SEI.[7–9,22–24] A plethora of studies probing the mechanism of decomposition of different classes of electrolytes on the electrode surface were reported over the years.[18,25–31] These studies indicate that the kinetics of formation and the structure of SEI is largely determined by (i) the interaction between the electrode surface and the electrolyte[32,33] and (ii) the interaction between the ions and solvents that are part of the electrolyte.[34–36] Experimental and computational studies over the years suggest that the formation of SEI in LIBs and post-LIBs involves the reduction of the electrolyte by accepting electrons from the anode surface followed by consecutive bond cleavages.[18,25–31]

[a] M. C. Madhusudhanan, S. Nair
School of Chemistry, Indian Institute of Science Education and Research Thiruvananthapuram
Thiruvananthapuram, Kerala 695551, India
[b] S. A. Kumar
School of Physics, Indian Institute of Science Education and Research Thiruvananthapuram
Thiruvananthapuram, Kerala 695551, India
[c] N. Srinivasan, M. Buragohain, Dr. S. Kunnikuruvan
Department of Chemistry, Indian Institute of Technology Madras
Chennai, Tamil Nadu 600036, India
E-mail: soorajk@iitm.ac.in

Supporting information for this article is available on the WWW under https://doi.org/10.1002/batt.202200430

Research Article
doi.org/10.1002/batt.202200430
Chemistry Europe
European Chemical Societies Publishing

Since SEI formation is initiated by the electron transfer from the Fermi level of the anode to the lowest unoccupied molecular orbital (LUMO) of the electrolyte, the factors which stabilize the LUMO of the electrolyte were expected to improve the kinetics of the reductive decomposition. Studies indicate that the LUMO of the electrolyte is more stable as compared to that of the solvent and is ascribed to the presence of stabilizing ion-solvent interactions in electrolytes.[10,29,34,37] Therefore, the change in the LUMO energy (ΔE_{LUMO}) of the solvent due to the ion-solvent complex formation was considered as a measure of the feasibility of SEI formation by the reductive decomposition of these complexes.[34,37] However, the reduction of the electrolyte by accepting electrons from the metal surface is expected to be a fast process as the working potential of metal anodes is above the reduction potential of the commonly used electrolytes. According to previous computational studies, the fast reduction process is followed by comparatively slow bond cleavage steps.[30,38–40] Correspondingly, comparing the values of critical reactivity parameters that control the slow bond cleavage steps would be more crucial than comparing the ΔE_{LUMO} of electrolytes for predicting their reductive decomposition kinetics.

In addition to reductive decomposition, anion decomposition of the salts that are part of the electrolyte and the decomposition of solvent molecules by the nucleophilic attack of anions generated by the salt or solvent decomposition are also known to contribute to SEI structure.[41–50] Though such reactions were comparatively less explored with regard to SEI formation, the presence of metal halides and fluorinated components of SEI found in experiments indicates that a clear understanding of the mechanism and the factors affecting such reactions are vital.

Herein, we have employed DFT-based electronic structure calculations and free energy computations to determine critical chemical reactivity descriptors that can provide vital information on the kinetics of SEI formation in presence of some of the commonly used electrolytes in LIBs and post-LIBs. This study highlights the importance of ion-solvent combinations in determining the kinetics of SEI formation as well as approaches to design new solvents to tune the SEI formation kinetics.

Results and Discussion

In order to identify the chemical reactivity descriptors that can provide insights into the kinetics of the reductive decomposition of the electrolytes, we employed DFT-based electronic structure calculations and free energy computations for some of the commonly used electrolytes in LIBs and post-LIBS. Herein, 45 different electrolytes or ion-solvent complexes that are formed between 5 different cations and 9 different solvents (Figure 1) were considered initially. The cations considered include 3 monovalent cations (Li^+, Na^+, K^+) and 2 divalent cations (Ca^{2+} and Mg^{2+}) and the solvents include 4 cyclic carbonates (ethylene carbonate (EC), einylene carbonate (VC), propylene carbonate (PC) and fluoro-ethylene carbonate (FEC)), 3 linear carbonates (diethyl carbonate (DEC), dimethyl carbonate (DMC) and ethyl methyl carbonate (EMC)) and 2 ethers (1,2-dimethoxyethane (DME) and 1,3 dioxalane (DOL)). The free energy barriers for the reductive decomposition of these electrolytes and the values of different possible chemical reactivity descriptors were then computed. We noted that the mechanism of the reductive decomposition of some of the ion-solvent complexes involving different classes of solvents and ions considered here are well scrutinized in previous studies[30,51–53] Thus, the energetically favourable mechanistic routes identified in previous studies for different classes of solvents were considered in this work.

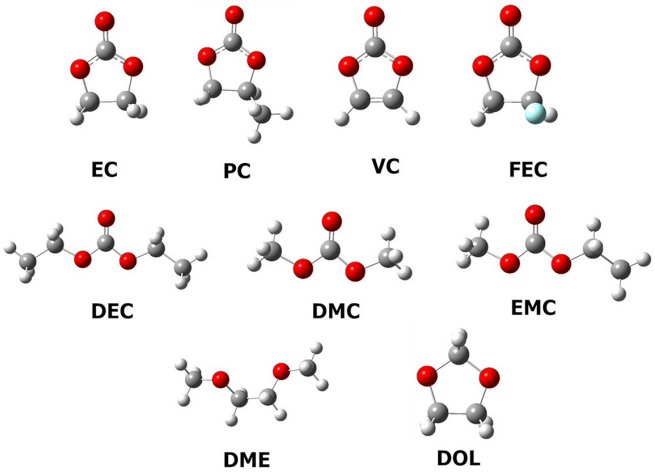

Figure 1. Optimized structures of the solvent molecules. Atom color codes: C (Grey), O (Red), H (White), F (Blue).

According to previous studies, the reductive decomposition of carbonates and ether-based ion-solvent complexes involves a rate-determining C–O bond cleavage step.[30] Therefore, the feasibility of the reductive decomposition of the electrolytes was analyzed by comparing the free energy barriers ($\Delta G^{\ddagger}_{RDS}$) for the rate-determining steps (RDS). The mechanistic schemes followed in this work are given in Figure 2. The optimized structures of the ion-solvent complexes before and after reduction and the transition state structures (TS) for the C–O bond cleavage are provided in the SI (Figures S21–S35).

The optimized geometries of ion-solvent complexes of cyclic carbonates reveal a preferential binding of all the considered cations to the carbonyl oxygen of these solvents. A comparison of $\Delta G^{\ddagger}_{RDS}$ of different cyclic carbonate-based ion-solvent complexes suggests that except for K-ion complexes the $\Delta G^{\ddagger}_{RDS}$ follows the order EC < PC < FEC < VC (Figure 3a and Table S5) irrespective of the cations involved. For K-ion complexes, the $\Delta G^{\ddagger}_{RDS}$ follows the order EC ≈ FEC < PC < VC.

It can also be seen from Figure 3a that the $\Delta G^{\ddagger}_{RDS}$, of ion-solvent complexes involving Li-ions, is lower when compared with the ion-solvent complexes of other cations. This suggests a faster decomposition of Li ion-solvent complexes compared to others. In addition, we also noted a higher $\Delta G^{\ddagger}_{RDS}$ for the ion-solvent complexes involving divalent cations compared to their monovalent counterparts.

As in cyclic carbonates, the cations were found to be bounded to the carbonyl oxygen for all the ion-linear carbonate

Research Article
doi.org/10.1002/batt.202200430
Chemistry Europe
European Chemical Societies Publishing

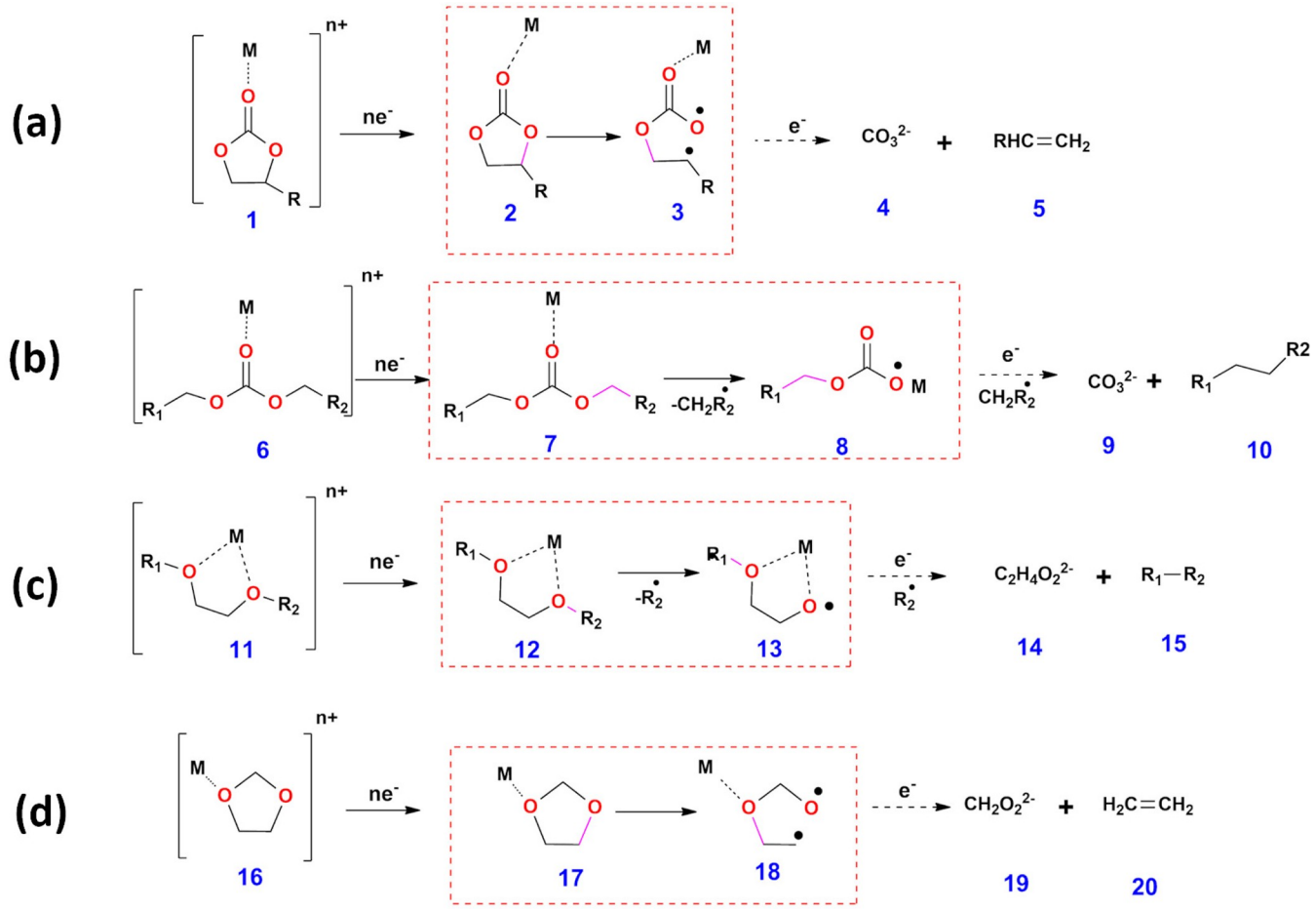

Figure 2. The mechanism of reductive decomposition for the ion-solvent complex formed between mono- and divalent-cations and (a) cyclic carbonates,[30,51,52] (b) linear carbonates,[30,54] (c) linear ethers,[29] and (d) cyclic ethers.[27,29] The rate-determining C–O bond cleavage steps are shown in red dotted boxes.

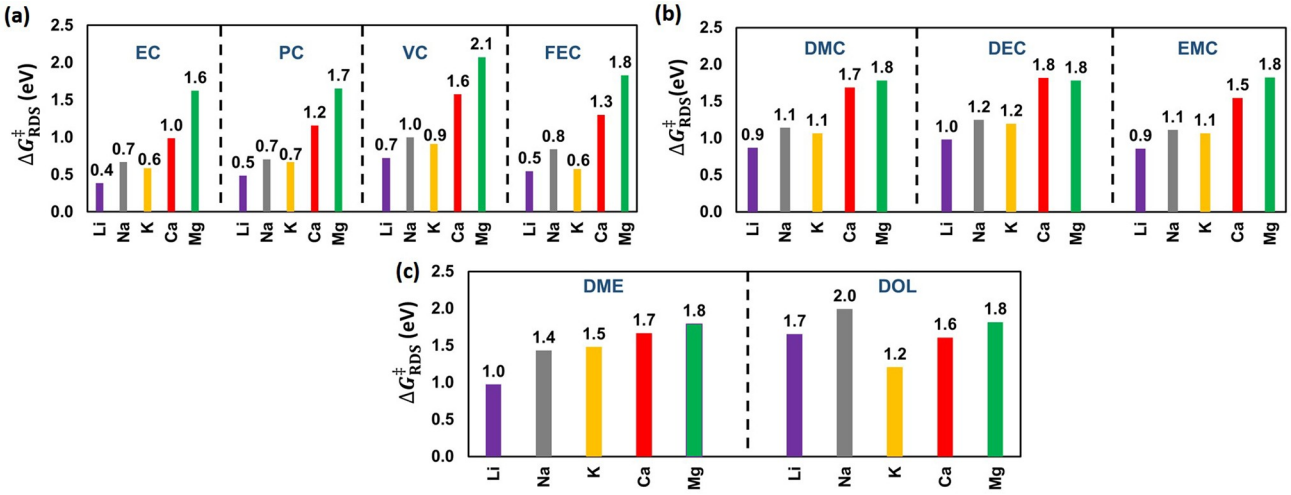

Figure 3. $\Delta G^{\ddagger}_{RDS}$ (in eV) for the rate-determining C–O bond cleavage steps (see Figure 2) for the ion-solvent complexes formed between (a) cyclic carbonates, (b) linear carbonates, and (c) ethers and mono- and divalent-cations.

solvent complexes except for the Mg ion-solvent complexes. In Mg ion-solvent complexes, the Mg^{2+} ions were found to be bounded to the ester oxygen forming a five-member cyclic ring-like structure. Analysis of $\Delta G^{\ddagger}_{RDS}$ (Figure 3b) suggests a comparable barrier for the rate-determining C–O bond cleavage (step **7**→**8** in Figure 3b) for the ion-solvent complexes

formed between a particular cation with varying linear carbonate solvents. As in cyclic carbonates, an increase in $\Delta G^{\ddagger}_{RDS}$ of ion-solvent complexes on going from mono- to divalent-cations was observed in linear carbonates also.

The $\Delta G^{\ddagger}_{RDS}$ of ethers (Figure 3c) was found to be higher than that of cyclic and linear carbonates for the monovalent ion-solvent complexes. Whereas for the divalent ion-solvent complexes, the $\Delta G^{\ddagger}_{RDS}$ were comparable to that of carbonates. Unlike other ion-solvent complexes, the divalent ion complexes of DOL were found to have a lower $\Delta G^{\ddagger}_{RDS}$ as compared to its complexes with Li and Na ions.

Analysis of $\Delta G^{\ddagger}_{RDS}$ for all the 45 complexes considered here indicates that the ether complexes undergo a slower reductive decomposition than the carbonates. This could be attributed to the stabilization of the radical transition state of cyclic and linear carbonates due to the neighbouring carboxylate group compared to ethers, which are devoid of such stabilization. The lower $\Delta G^{\ddagger}_{RDS}$ of the cyclic carbonates (for a particular cation) as compared to linear carbonates can be ascribed to the comparatively higher stability of the 2^0 radical TS in the RDS as compared to the 1^0 radical TS involved in the RDS of the linear carbonates.

The trend in $\Delta G^{\ddagger}_{RDS}$ discussed above was found to be in good agreement with the experimental reports. The NMR studies of Zhuang et al. and gas chromatographic studies of Onuki et al. support faster decomposition of cyclic carbonates as compared to linear carbonates.[55,56] C-13 NMR and XPS studies of Lee et al. on the decomposition behavior of linear carbonates in the presence of FEC on Na metal anodes indicate a faster decomposition of FEC compared to linear carbonates such as DEC and DMC. These results are consistent with the lower $\Delta G^{\ddagger}_{RDS}$ of cyclic carbonates as compared to linear carbonates.[57] The faster decomposition of DME in comparison to DOL observed for the Li-ion complexes was consistent with the ESI-MS spectroscopy and computational studies by Liu et al.[27] FTIR spectroscopic, elemental, and XPS analysis by Fan et al. noted that the SEI layer formed in the K-ion battery is devoid of organic compounds in presence of DME, whereas such compounds were observed in presence of EC-EMC mixture.[58] This is consistent with the slow reductive decomposition of ion-solvent complexes involving ethers as compared to linear and cyclic carbonates observed in this study.

Further, we analyzed the relation between the $\Delta G^{\ddagger}_{RDS}$ and the values of various chemical reactivity descriptors for individual ions and solvents that form the 45 ion-solvent complexes studied here. The chemical reactivity descriptors considered here are chemical potential (μ), electronegativity (χ), chemical hardness (η), electrophilicity (ω), electron affinity (A), and ionization potential (I). The values of these descriptors are related to the frontier orbital energies by Equations (5–10). Such reactivity descriptors were used widely for predicting the chemical reactivity in previous studies.[59–63] In addition to these 6 chemical reactivity descriptors, we also analyzed the correlation of $\Delta G^{\ddagger}_{RDS}$ with ΔE_{LUMO} and binding energy of the ion-solvent complexes, which are used in previous studies to predict the reductive decomposition behavior (see Section S1 in SI).[34,59,64,65]

The correlation between $\Delta G^{\ddagger}_{RDS}$ and the reactivity descriptors was then analyzed by constructing a contour plot between $\Delta G^{\ddagger}_{RDS}$ of the ion-solvent complexes and the values of the chemical reactivity descriptors for individual ions and solvents that constitute the ion-solvent complexes (Figure 4). It is evident from Figure 4 that among the 6 chemical reactivity descriptors considered here, only the contour plots of electron affinity (A) and electrophilicity (ω) are composed of distinct regions that differentiate the ion-solvent complexes with slow reductive decomposition kinetics (high $\Delta G^{\ddagger}_{RDS}$) from those with faster kinetics (low $\Delta G^{\ddagger}_{RDS}$; deep blue regions in Figure 4). It is to be mentioned here that a faster reductive decomposition is expected for all those complexes having $\Delta G^{\ddagger}_{RDS}$ less than 0.5 eV, which corresponds to a timescale of about 10^{-5} seconds (Table S5 and Figure S19).

Figure 4a and 4b indicates that ion-solvent complexes that undergo a fast reductive decomposition constitute ions of comparatively low electrophilicity (<22 eV; among ions) and electron affinity (<8 eV; among ions), and solvents having comparatively high electrophilicity (>2.8 eV; among solvents) and electron affinity (>0.3 eV; among solvents). Here, the electron affinity as well as the electrophilicity of the ions were compared among the ions and that of solvents were compared among the solvents. We noted in passing that the trend in the values of the different chemical reactivity descriptors is in line with the experimental and computational studies reported previously.[34,60–64,66]

Since both electron affinity and electrophilicity are related to the tendency of the molecule to accept the electron, the above results suggest that the ion-solvent complexes formed between ions having a low electron-accepting tendency and a solvent having a high electron-accepting tendency will undergo a faster reductive decomposition. We also noted a qualitative increase in the negative potential near the solvent region in the TS of complexes formed between cations having high electron affinity/electrophilicity and solvents with low electron affinity/electrophilicity as indicated by the electrostatic potential maps (Figure 5). This is also in agreement with the higher negative charge on the C and O atoms of the C–O bond, which undergoes cleavage in the RDS, for the ion-solvent complexes involving divalent cations (Table S11). Since the radicals were expected to localize in the solvent part of the ion-solvent complexes such a negative potential is expected to destabilize the radicals, which in turn could be responsible for the higher $\Delta G^{\ddagger}_{RDS}$ values for the complexes of divalent cations as compared to that of monovalent ion complexes.

As mentioned earlier, ΔE_{LUMO} and binding energy of the ion-solvent complexes were suggested as reactivity descriptors for the reductive decomposition of electrolytes in previous studies.[37] However, these studies were focused on the change in energy of LUMO of the solvents on the formation of ion-solvent complexes and not on the free energy barriers for the reductive decomposition of these complexes. The analysis of the correlation of $\Delta G^{\ddagger}_{RDS}$ with ΔE_{LUMO} and binding energy indicates a poor correlation for ion-solvent complexes formed between a particular cation and different solvents (Figures S15 and S16). Such a poor correlation was also observed for other

Research Article
doi.org/10.1002/batt.202200430
Chemistry Europe
European Chemical Societies Publishing

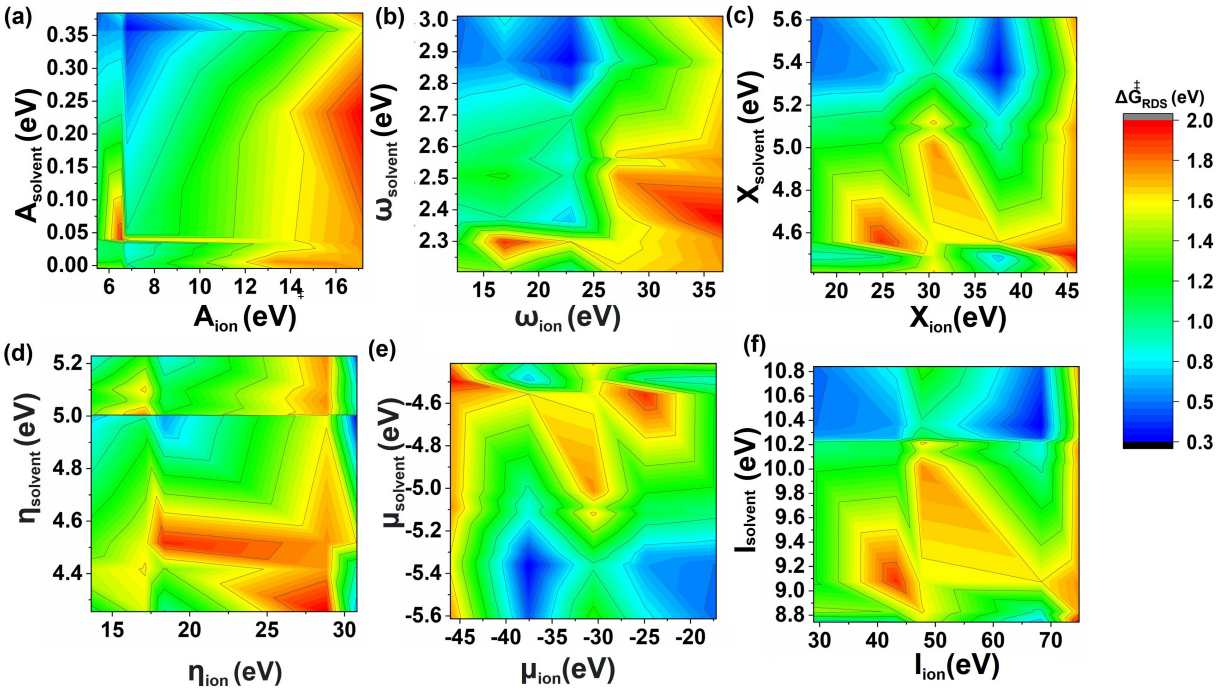

Figure 4. Contour plots of (a) electron affinity (*A*), (b) electrophilicity (ω), (c) electronegativity (χ), (d) chemical hardness (η), (e) chemical potential (μ), and (f) ionization potential (*I*) of the ions (X-axis) and solvents (Y-axis) plotted against $\Delta G^{\ddagger}_{RDS}$ for the reductive decomposition of the ion-solvent complexes considered.

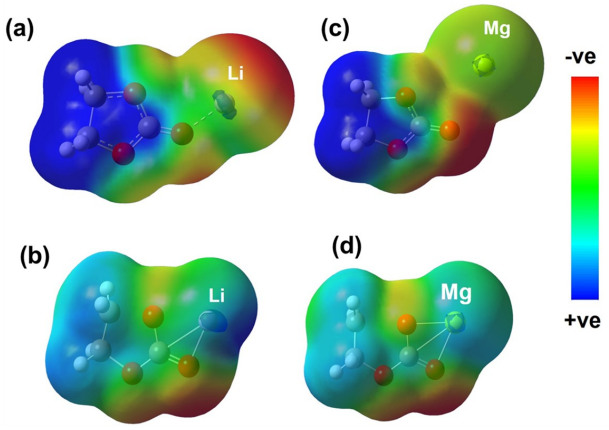

Figure 5. Electrostatic potential maps (isovalue: 0.001) of the reactant and transition state structures for the rate-determining C–O bond cleavage step for the (a, b) Li and (c, d) Mg ion complexes of EC (Figure 2).

reactivity descriptors (Figures S13, S14, and S17) when the correlation between $\Delta G^{\ddagger}_{RDS}$ and values of the descriptors for the ion-solvent complexes was analyzed. This clearly indicates that the electron affinity and electrophilicity of the individual ions and solvents can provide more insights into the reductive decomposition of the electrolytes as compared to the ion-solvent complexes. However, an improved correlation was observed while analyzing the correlation of ΔE_{LUMO} for individual solvents with varying cations (Figures S7–S12) for cyclic and linear carbonates and this is consistent with previous studies.[37]

It was found that the $\Delta G^{\ddagger}_{RDS}$ of some of the moderately bound (binding energy of 1–2 eV; Figure S18) ion-solvent complexes are less than 0.5 eV. However, all these complexes are formed between ions with low electron affinity and electrophilicity (among ions) and solvents having comparatively high electron affinity and electrophilicity (among solvents). These results also suggest that electron affinity and electrophilicity are more suitable and general reactivity descriptors for predicting the kinetics of the reductive decomposition of ion-solvent complexes as compared to ΔE_{LUMO} and binding energy of these complexes. The ΔE_{LUMO} and the trend in the binding energy of the different ion-solvent combinations considered here are also consistent with previous studies (Section S1 in SI).[37]

To further affirm the validity of electron affinity and electrophilicity as suitable descriptors to predict the reductive decomposition of ion-solvent complexes, we analyzed the reductive decomposition behavior of 8 new ion-solvent complexes. Here, the complexes were considered to be formed between 4 solvents (tert-butyl ethylene carbonate (TEC), trifluoro propylene carbonate (TFPC),[67] flourinated Dimethyl carbonate (F-DMC),[68] and diethoxy ethane (DEE))[69,70] and 2 cations (Li^+ and Ca^{2+}). These solvents belong to the class of cyclic carbonates, linear carbonates, and ethers respectively (Figure 6), and are used in LIBs and post-LIBs.

The electron affinity and electrophilicity of the individual ions and solvents, and the $\Delta G^{\ddagger}_{RDS}$ for the reductive decomposition of the ion-solvent complexes formed between these ions and solvents were then computed. Here also, the mechanisms shown in Figure 2 were followed for the respective class of solvents. It was found that the complementing electron affinity/electrophilicity behavior, the values of these descriptors

Research Article
doi.org/10.1002/batt.202200430
Chemistry Europe
European Chemical Societies Publishing

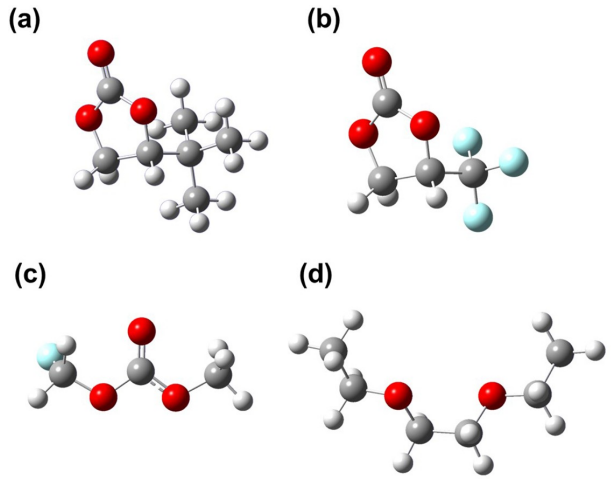

Figure 6. Optimized structures of the solvents (a) TEC, (b) TFPC, (c) F-DMC, and (d) DEE.

for the ions and these solvents, and their correlation with the $\Delta G^{\ddagger}_{RDS}$ are the same as that observed for the 45 ion-solvent complexes discussed earlier (Figure 7, Table 1 and Table S6).

In addition to the reductive decomposition reactions discussed above, we also studied other crucial reactions such as anion decomposition and nucleophilic substitution reactions that are known to contribute to SEI formation.[41–46] Experiments that scrutinize the components of SEI suggest the presence of metal halides (e.g. LiF) and HF. According to these studies, anion decomposition could be responsible for their formation.[47–50]

To analyze the correlation between the values of the chemical reactivity descriptors and the free energy barriers for anion decomposition reactions of salts that leads to metal halides, we calculated the $\Delta G^{\ddagger}_{RDS}$ for the metal halide formation from 12 salts formed between 4 anions (PF_6^-, AsF_6^-, ClO_4^-, and $TFSI^-$ (Bis(trifluoromethane) sulfonimide)) and three cations (Li^+, Na^+, and K^+) (Figures S38–S44). The reactions considered here are given in Equations (1–4) and we followed the mechanism reported in previous studies.[71–73] It is to be mentioned here that while studying the metal halide formation from $TFSI^-$, we studied only the initial decomposition, assuming the formation of MSO_2CF_3 as the RDS.

$$MPF6_6 \rightarrow MF + PF_5 \quad (1)$$

$$MClO_4 \rightarrow MCl + ClO_3 \quad (2)$$

$$MAsF_6 \rightarrow MF + AsF_5 \quad (3)$$

$$MTFSI \rightarrow MSO_2CF_3 + M_2NSO_2CF_3$$
$$MSO_2CF_3 \rightarrow MF + M_2O \quad (4)$$

where M = Li, Na, K.

The $\Delta G^{\ddagger}_{RDS}$ calculated for the formation of metal halides by anion decomposition suggests that the formation of metal fluorides is faster as compared to metal chlorides in presence of Li^+ and Na^+ ions (Figure 8 and Table S14). However, we noted a lower $\Delta G^{\ddagger}_{RDS}$ for KCl formation as compared to KF formation (Table S14).

The trend in $\Delta G^{\ddagger}_{RDS}$ observed in this study is consistent with the experimental studies based XPS depth profile analysis, F-19 NMR, and conductometric analysis performed by different groups (Table 2).[41,72,74–76] We noted in passing that the binding energies of the salt complexes are in line with the dissociation constants of Li-salts reported in previous experimental studies (Table S13).[77,78] In addition, we also noted that $\Delta G^{\ddagger}_{RDS}$ for HF formation from the anion decomposition product indicates was found to be comparable (0.86 eV by reaction between PF_5 and H_2O) to that of anion decomposition (Figure S47, Table S16). This is also consistent with the experimental identification of HF formation during SEI formation.[46]

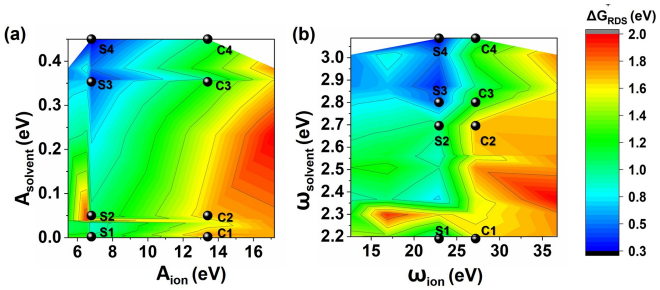

Figure 7. Contour plots of (a) electron affinity (*A*) and (b) electrophilicity (ω) of the ions (X-axis) and solvent (Y-axis) plotted against $\Delta G^{\ddagger}_{RDS}$ for the reductive decomposition of the 45 + 8 ion-solvent complexes considered. The points S1–S4 correspond to the ion-solvent complexes of DEE, F-DMC, TEC, and TFPC, respectively, with Li-ion. The points C1–C4 represent ion-solvent complexes of DEE, F-DMC, TEC, and TFPC, respectively, with Ca ion.

Table 1. The calculated values (in eV) of different reactivity descriptors for the solvents, TEC, TFPC, F-DMC, and DEE, and $\Delta G^{\ddagger}_{RDS}$ (in eV) for the decomposition of the ion-solvent complexes of these solvents with Li and Ca ions. The cutoff values of these descriptors for solvents ($d_{solvent}$) and ions (d_{ion}) whose combination results in ion-solvent complexes with $\Delta G^{\ddagger}_{RDS} < 0.5$ eV obtained from the analysis of the 45 ion-solvent complexes considered initially are also given (Table S6).

Reactivity descriptor	TEC	TFPC	F-DMC	DEE	$d_{solvent}$	d_{ion}
Chemical potential	−5.22	−5.67	−5.33	−4.37	< −5.2	−35 to −40 and −23 to −20
Electronegativity	5.22	5.67	5.33	4.37	> 5.2	35 to 40 and 20 to 23
Electron affinity	0.35	0.45	0.05	0.002	> 0.3	< 8
chemical hardness	4.86	5.22	5.28	4.37	> 4.8	35
electrophilicity index	2.8	3.08	2.69	2.19	> 2.8	< 22
ionization potential	10.09	10.90	10.62	8.75	> 10.2	30–35 and 65–70
$\Delta G^{\ddagger}_{RDS}$ (Li^+)	0.49	0.31	1.02	1.01		
$\Delta G^{\ddagger}_{RDS}$ (Ca^{2+})	1.21	1.02	1.73	1.69		

Research Article
doi.org/10.1002/batt.202200430
Chemistry Europe
European Chemical Societies Publishing

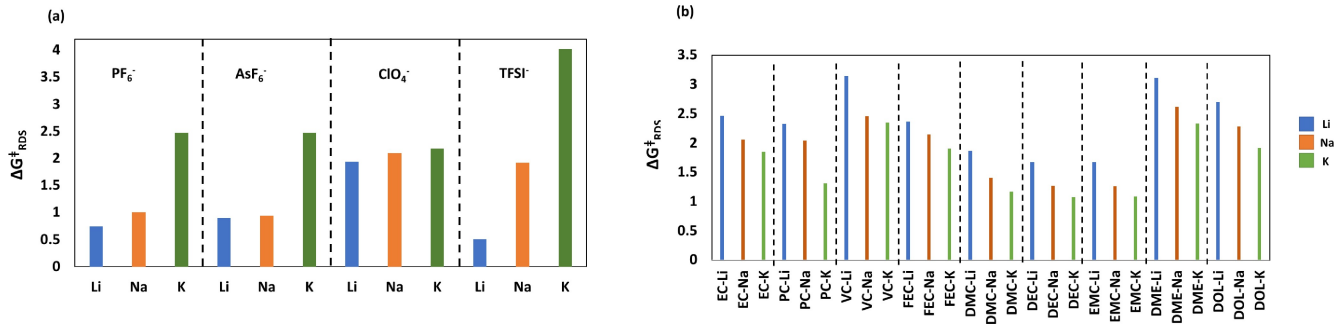

Figure 8. $\Delta G^{\ddagger}_{RDS}$ (in eV) for (a) anion decomposition of salts and (b) C–O bond cleavage by nucleophilic attack of F^- on ion-solvent complexes.

Table 2. Comparison of the trends in the kinetics of reductive decomposition and anion decomposition of salts with previous experimental studies.

Type	Trend observed in current work	Trend observed in experiments	Method used in experiment	Refs.
Feasibility of reductive decomposition of solvents	Cyclic carbonates (EC, PC, VC, FEC) > Linear carbonates (DMC, EMC, DEC) > Ethers (DOL, DME) in presence of Li^+ and Na^+ ions	EC > EMC in presence of Li salt	^{1}H and C-13 NMR	[55]
		EC > DEC in presence of Li salt	Gas Chromatography	[56]
		EC, PC > DEC, DMC	C-13 NMR and ESI-MS	[84]
		FEC > DEC and DMC in presence of Na salt	C-13 NMR	[57]
		DOL > DME in presence of Li salt	ESI-MS and XPS Spectra	[27,58]
			Gas Chromatography and Mass spectroscopy	[6]
Feasibility of anion decomposition	$PF_6^- > ClO_4^- > TFSI^-$ in presence of Na^+ ion	$PF_6^- > ClO_4^- > TFSI^-$ in presence of Na + ion	Surface and depth profiling using XPS analysis	[72,74]
	$PF_6^- \approx TFSI^-$ in presence of Li^+ ion	$PF_6^- \approx TFSI^-$ in presence of Li^+ ion	Electrochemical cycling, TEM, XPS, FTIR and F-19 NMR	[75]
	$PF_6^- > TFSI^-$ in presence of K^+ ion	$PF_6^- > TFSI^-$ in presence of K^+ ion	DRT[a] and XPS spectra	[85]
	$ClO_4^- < PF_6^-$ in presence of Li^+ ion	$ClO_4^- < PF_6^-$ in presence of Li^+ ion	Conductometric analysis	[81]

The correlation between various chemical reactivity descriptors and $\Delta G^{\ddagger}_{RDS}$ were further scrutinized by analyzing the contour plot between the values of these descriptors for cations and anions that constitute the salt molecules considered here together with $\Delta G^{\ddagger}_{RDS}$. As in the case of reductive decomposition reactions, electron affinity and electrophilicity were found to be valid descriptors for this reaction also as indicated by the well-separated regions corresponding to low and high $\Delta G^{\ddagger}_{RDS}$ values (Figure 9, Tables S7 and Table S12).

It can be seen from Figure 9(a) that anion decomposition is more facile ($\Delta G^{\ddagger}_{RDS}$ between 0.5–0.8 eV) for salts containing cations with higher electron affinity (> 6.6 eV) irrespective of the anions. Figure 9(b) indicate that cations with electrophilicity values greater than 20 eV undergo a faster metal halide formation compared to others irrespective of the anions present in the salt complex. These results are in agreement with the identification of metal fluorides as a part of SEI in experiments that looked at the SEI structure in Li, Na-ion batteries.[75,76,79–81]

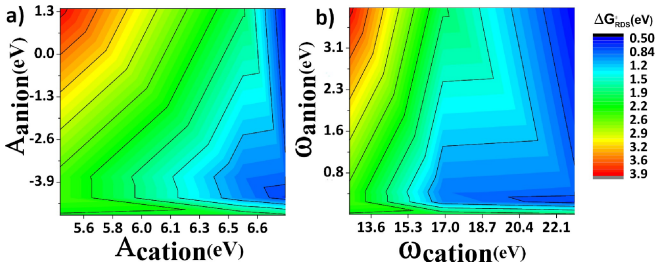

Figure 9. Contour plots of (a) electron affinity and (b) electrophilicity of the cations (X-axis) and anions (Y-axis) plotted against $\Delta G^{\ddagger}_{RDS}$ for the anion decomposition reaction.

Further, we have also studied the electrolyte decomposition by the C–O bond cleavage due to the nucleophilic attack of F^- ion. Here, F^- ion can be formed by the anion decomposition of salt molecules. Such reactions could also be responsible for forming halogenated products and acids such as HF found in experiments.[45]

To understand the role of nucleophilic addition reactions in the SEI formation, we considered the initial steps of decomposition of 27 ion-solvent complexes, which represent 27 electrolytes, by the nucleophilic attack by F^- ion. Here, the electrolytes or the ion-solvent complexes are formed between 9 different solvents (EC, PC, VC, FEC, DMC, DEC, EMC, DOL, and DME) and 3 cations (Li^+, Na^+, and K^+).

The $\Delta G^{\ddagger}_{RDS}$ for the nucleophilic attack-assisted C–O bond cleavage was then calculated for all 27 electrolytes. The mechanism followed in this work is shown in Figure 10.

Analysis of $\Delta G^{\ddagger}_{RDS}$ indicated faster C–O bond cleavage reactions for K^+ ion-based electrolytes as compared to Li^+ and Na^+ ion solvent complexes (Figure 8(b) and Table S17). The slower decomposition or higher $\Delta G^{\ddagger}_{RDS}$ of K^+ ion DME complex as compared to K ion complexes of EC and PC solvents is in

Research Article
doi.org/10.1002/batt.202200430
Chemistry Europe
European Chemical Societies Publishing

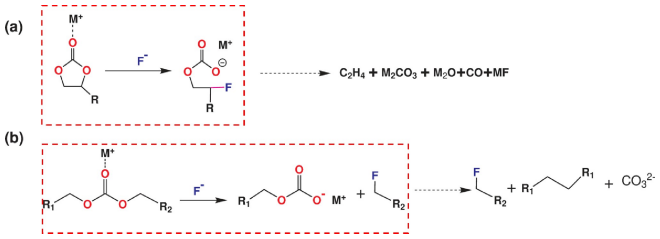

Figure 10. The mechanism of C–O bond cleavage by the nucleophilic attack of F^- on (a) cyclic carbonates and (b) linear carbonates. The elementary reaction steps studied in this work are shown within red dotted boxes. A mechanism similar to the cyclic and linear carbonates was followed for cyclic and linear ethers.

line with the experimental studies of Hosaka et al. and theoretical studies of Yoshida et al., where they suggested a slow decomposition of the K ion-DME complex.[82,83] We noted that $\Delta G^{\ddagger}_{RDS}$ for the nucleophile-assisted C–O bond cleavage is relatively higher as compared to the reductive decomposition and anion decomposition.

The correlation between the chemical reactivity descriptors and the $\Delta G^{\ddagger}_{RDS}$ was then analysed by constructing the contour plot between the values of these descriptors for individual ions and solvents together with $\Delta G^{\ddagger}_{RDS}$ (Figure 11, Tables S6, S7 and S17).

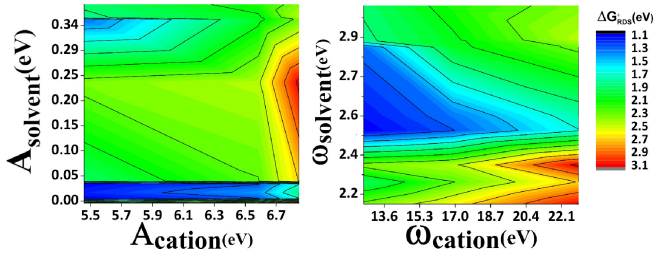

Figure 11. Contour plots of electron affinity (left) and electrophilicity (right) of ions (X-axis) and solvents (Y-axis) plotted against $\Delta G^{\ddagger}_{RDS}$ for the decomposition of the ion-solvent complex by the nucleophilic attack of F^- ion.

As indicated by Figure 11, electron affinity and electrophilicity are good descriptors for the F^- ion-assisted decomposition of ion-solvent complexes also. It can be seen from Figure 11(a) that the electrolytes composed of solvents with low electron affinity (between 0 and 0.03 eV) undergoes a comparatively faster C–O bond cleavage irrespective of the cation present in the electrolyte. We noted that the solvents with electrophilicity values between 0 and 0.03 eV belongs to the linear carbonates. Similarly, analysis of Figure 11(b) indicates that ions with electrophilicity value 13–15 eV and solvents with 2.5–2.8 eV undergo a comparatively faster decomposition.

The trends in the free energy barriers for different classes of reactions and the chemical reactivity descriptor analysis were found to explain many experimental observations as discussed (*vide supra*) above. A detailed comparison between the observations made in this study and experiments is given in Table 2. A schematic representation of the feasibility of the formation of the components of SEI from different electrolytes and salts is provided in Figure 12.

The above results indicate that electron affinity and electrophilicity are suitable chemical reactivity descriptors for predicting the kinetics of different reactions that contribute to SEI formation in metal anode-based batteries. Thus, they can be used as a measure to predict the kinetics of the SEI formation involving an arbitrary electrolyte before their practical applications in experiments, especially carbonate and ether-based electrolytes. Since the electron affinity and electrophilicity of salts and solvents are their inherent properties, one can modulate the kinetics of reductive decomposition of the electrolyte on the electrode surface by chemically modifying them. As the electron affinity depends only on the LUMO energies and electrophilicity on the HOMO and LUMO energies,

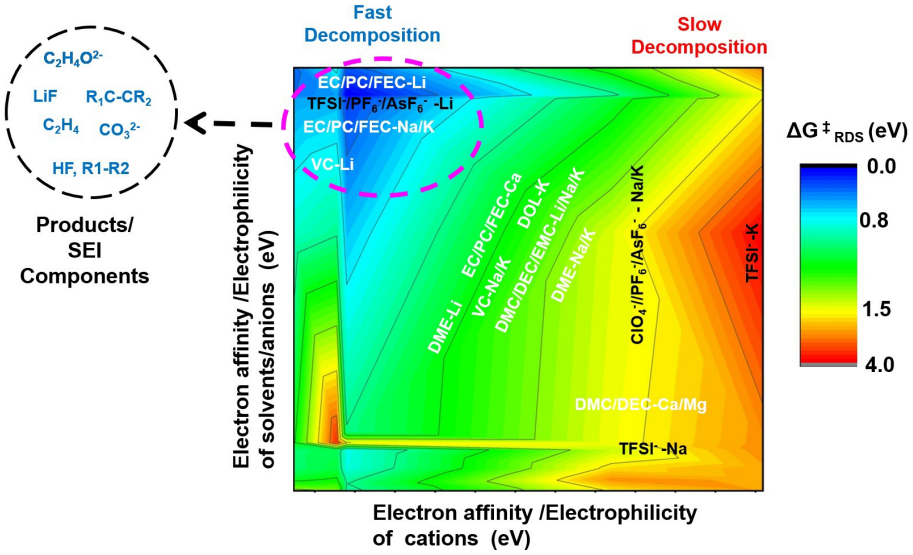

Figure 12. A schematic representation of the feasibility of the formation of different SEI components from the electrolytes and salts that are considered in this work.

Research Article
doi.org/10.1002/batt.202200430
Chemistry Europe
European Chemical Societies Publishing

any chemical modifications that can influence the frontier orbital energies of the salts and solvents are expected to affect the SEI formation kinetics.

Conclusion

In this work, we employed DFT-based electronic structure calculations and free energy computations to identify potential chemical reactivity descriptors that can bring light to the kinetics of SEI formation. For this, we considered 3 different classes of reactions (reductive decomposition of ion-solvent complexes, anion decomposition, and anion-assisted decomposition of ion-solvent complexes) that are known to contribute to the SEI formation.

For identifying suitable chemical reactivity descriptors for reductive decomposition reactions a set of 45 ion-solvent complexes that are formed between 5 cations (Li^+, Na^+, K^+, Ca^{2+}, and Mg^{2+}) and 9 solvents belong to the class of cyclic carbonates, linear carbonates, and ethers were considered. The free energy barriers for the reductive decomposition of these ion-solvent complexes were then analyzed together with the values of different chemical reactivity indices for individual ions and solvents that constitute these complexes. This analysis indicates electron affinity and electrophilicity of the individual ions and solvents that constitute the electrolyte as the suitable descriptors that can distinguish between ion-solvent complexes having slow and fast decomposition or SEI formation kinetics. The validity of electron affinity and electrophilicity as suitable descriptors were further affirmed by studying the decomposition kinetics of 8 additional ion-solvent complexes that are formed between some of the recently reported solvents and Li and Ca ions. The results of this study suggest that the ion-solvent complex formed between ions having low electron affinity and electrophilicity as well as solvents having high electron affinity and electrophilicity are associated with faster reductive decomposition kinetics.

The free energy barrier calculations and analysis of various chemical reactivity descriptors for anion decomposition and anion-assisted ion-solvent decomposition also indicates the validity of electron affinity and electrophilicity as suitable chemical reactivity descriptors for these class of reactions also. Therefore, one can control the kinetics of these reactions by modulating the values of these reactivity descriptors either by the chemical modification of the solvents or by choosing an appropriate combination of ions and solvents. The relation between electrophilicity and electron affinity with the frontier orbital energies suggests that the chemical modifications that alter the frontier orbital energies will also affect the SEI formation kinetics. The results presented here are expected to have a large impact on the ongoing efforts in the development of high-performance Li and post-Li ion batteries by modulating the interfacial properties.

Computational Details

All calculations were performed using the Gaussian 16 suite of programs[86] at the M06-2X/6-31++G(d,p) level of theory.[87] Geometry optimization was performed employing the GEDIIS method as implemented in Gaussian 16 to determine the stationary state structures.[88] The Gibbs free energies of all the stationary points were calculated and the computed free energy values include the zero-point energy correction and thermal correction to enthalpy and entropy. The minima and transition state structures were confirmed by the absence and presence of the imaginary vibrational modes, respectively, in the normal mode analysis.

The values of 6 different chemical reactivity indices namely chemical potential (μ), electronegativity (χ), chemical hardness (η), electrophilicity (ω), electron affinity (A), and ionization potential (I) were determined using their relations (Equations (5–10)) with the frontier orbitals as follows:

$$-\varepsilon_{HOMO} = I \tag{5}$$

$$-\varepsilon_{LUMO} = A \tag{6}$$

$$\mu = \frac{(\varepsilon_{HOMO} + \varepsilon_{LUMO})}{2} \tag{7}$$

$$\eta = \frac{(\varepsilon_{LUMO} - \varepsilon_{HOMO})}{2} \tag{8}$$

$$\omega = \frac{\mu^2}{2\eta} \tag{9}$$

$$\chi = -\mu \tag{10}$$

The contribution of solvation to the free energy values computed was analyzed by employing the SMD implicit solvent model (Table S9).[89] We noted that Gibbs free energy of rate-determining step, $\Delta G^{\ddagger}_{RDS}$ and the critical reactivity parameters such as electrophilicity follow the same trend in both gas phase and solvent (See Section S6, Figures S5 and S6 in SI). Thus, for the comparison of $\Delta G^{\ddagger}_{RDS}$ and reactivity descriptors for different electrolytes, we have used the gas phase values unless otherwise specified.

Supporting Information

The details of LUMO and binding energy calculations, solvent correction, free energies, values of reactivity descriptors, figures of all the optimized structures of minima and transition states, and Cartesian coordinates of all the structures are provided.

Acknowledgements

SK thanks the Department of Science and Technology (DST), India for the INSPIRE faculty fellowship. MCM, SN, and NS thank DST for the funding of their project associate positions through the INSPIRE faculty fellowship. The authors thank IISER Thiruvananthapuram and IIT Madras for the high-performance computing (HPC) facilities.

Conflict of Interest

No conflict of interest to declare.

Data Availability Statement

The data that support the findings of this study are available in the supplementary material of this article.

Keywords: chemical reactivity descriptors · density functional theory · lithium-ion batteries · post-lithium-ion battery · reaction mechanism · solid-electrolyte interface

[1] F. Wu, J. Maier, Y. Yu, *Chem. Soc. Rev.* **2020**, *49*, 1569.
[2] M. Li, J. Lu, Z. Chen, K. Amine, *Adv. Mater.* **2018**, *30*, 1800561.
[3] A. Ponrouch, M. R. Palacín, *Philos. Trans. R. Soc. London Ser. A* **2019**, *377*, 20180297.
[4] P. Canepa, G. Sai Gautam, D. C. Hannah, R. Malik, M. Liu, K. G. Gallagher, K. A. Persson, G. Ceder, *Chem. Rev.* **2017**, *117*, 4287.
[5] X. Xiong, Q. Zhou, Y. Zhu, Y. Chen, L. Fu, L. Liu, N. Yu, Y. Wu, T. van Ree, *Energy Fuels* **2020**, *34*, 10503.
[6] J. Chen, H. Yang, X. Zhang, J. Lei, H. Zhang, H. Yuan, J. Yang, Y. Nuli, J. Wang, *ACS Appl. Mater. Interfaces* **2019**, *11*, 33419.
[7] C. Wei, Y. Tao, Y. An, Y. Tian, Y. Zhang, J. Feng, Y. Qian, *Adv. Funct. Mater.* **2020**, *30*, 2004613.
[8] D.-H. Liu, Z. Bai, M. Li, A. Yu, D. Luo, W. Liu, L. Yang, J. Lu, K. Amine, Z. Chen, *Chem. Soc. Rev.* **2020**, *49*, 5407.
[9] G. Wang, C. Chen, Y. Chen, X. Kang, C. Yang, F. Wang, Y. Liu, X. Xiong, *Angew. Chem. Int. Ed.* **2020**, *59*, 2055.
[10] M. Gauthier, T. J. Carney, A. Grimaud, L. Giordano, N. Pour, H.-H. Chang, D. P. Fenning, S. F. Lux, O. Paschos, C. Bauer, et al., *J. Phys. Chem. Lett.* **2015**, *6*, 4653.
[11] J. Yu, L. Zhao, Y. Huang, Y. Hu, L. Chen, Y.-B. He, *Front. Mater.* **2020**, *7*, 71.
[12] L. Wang, A. Menakath, F. Han, Y. Wang, P. Y. Zavalij, K. J. Gaskell, O. Borodin, D. Iuga, S. P. Brown, C. Wang, et al., *Nat. Chem.* **2019**, *11*, 789.
[13] X. Ren, P. Gao, L. Zou, S. Jiao, X. Cao, X. Zhang, H. Jia, M. H. Engelhard, B. E. Matthews, H. Wu, et al., *Proc. Natl. Acad. Sci. USA* **2020**, *117*, 28603.
[14] L. E. Camacho-Forero, P. B. Balbuena, *Phys. Chem. Chem. Phys.* **2017**, *19*, 30861.
[15] M. B. Pinson, M. Z. Bazant, *J. Electrochem. Soc.* **2012**, *160*, A243.
[16] E. Peled, *J. Electrochem. Soc.* **1979**, *126*, 2047.
[17] S. J. An, J. Li, C. Daniel, D. Mohanty, S. Nagpure, D. L. Wood III, *Carbon* **2016**, *105*, 52.
[18] A. Naji, J. Ghanbaja, B. Humbert, P. Willmann, D. Billaud, *J. Power Sources* **1996**, *63*, 33.
[19] Y. Jiang, B. Wang, P. Liu, B. Wang, Y. Zhou, D. Wang, H. Liu, S. Dou, *Nano Energy* **2020**, *77*, 105308.
[20] T. Zhou, Y. Zhao, M. El Kazzi, J. W. Choi, A. Coskun, *ACS Energy Lett.* **2021**, *6*, 1711
[21] Z. Lu, Z. Yang, C. Li, K. Wang, J. Han, P. Tong, G. Li, B. S. Vishnugopi, P. P. Mukherjee, C. Yang, W. Li, *Adv. Energy Mater.* **2021**, *11*, 2003811.
[22] D. Zhang, B. Li, S. Wang, S. Yang, *ACS Appl. Mater. Interfaces* **2017**, *9*, 40265.
[23] G. Agarwal, J. D. Howard, V. Prabhakaran, G. E. Johnson, V. Murugesan, K. T. Mueller, L. A. Curtiss, R. S. Assary, *ACS Appl. Mater. Interfaces* **2021**, *13*, 38816.
[24] D. Yu, H. Wang, W. Zhang, H. Dong, Q. Zhu, J. Yang, S. Huang, *Energy Storage Mater.* **2021**, *43*, 172.
[25] D. Aurbach, M. Daroux, P. Faguy, E. Yeager, *J. Electrochem. Soc.* **1993**, *140*, 922.
[26] N. Takenaka, Y. Suzuki, H. Sakai, M. Nagaoka, *J. Phys. Chem. C* **2014**, *118*, 10874.
[27] Q. Liu, A. Cresce, M. Schroeder, K. Xu, D. Mu, B. Wu, L. Shi, F. Wu, *Energy Storage Mater.* **2019**, *17*, 366.
[28] T. Husch, M. Korth, *Phys. Chem. Chem. Phys.* **2015**, *17*, 22799.
[29] L. E. Camacho-Forero, P. B. Balbuena, *J. Power Sources* **2020**, *472*, 228449.
[30] X. Liu, J. Zhou, Z. Xu, Y. Wang, *RSC Adv.* **2020**, *10*, 16302.
[31] J. M. Vollmer, L. A. Curtiss, D. R. Vissers, K. Amine, *J. Electrochem. Soc.* **2003**, *151*, A178.
[32] X. Yu, A. Manthiram, *Energy Environ. Sci.* **2018**, *11*, 527.
[33] C. Yan, R. Xu, Y. Xiao, J.-F. Ding, L. Xu, B.-Q. Li, J.-Q. Huang, *Adv. Funct. Mater.* **2020**, *30*, 1909887.
[34] X. Chen, H.-R. Li, X. Shen, Q. Zhang, *Angew. Chem. Int. Ed.* **2018**, *57*, 16643.
[35] X. Chen, X. Shen, B. Li, H.-J. Peng, X.-B. Cheng, B.-Q. Li, X.-Q. Zhang, J.-Q. Huang, Q. Zhang, *Angew. Chem. Int. Ed.* **2018**, *57*, 734.
[36] X. Chen, N. Yao, B.-S. Zeng, Q. Zhang, *Fundam. Res. Homogeneous Catal.* **2021**, *1*, 393.
[37] X. Chen, X. Shen, T.-Z. Hou, R. Zhang, H.-J. Peng, Q. Zhang, *Chem* **2020**, *6*, 2242.
[38] X. Zhang, R. Kostecki, T. J. Richardson, J. K. Pugh, P. N. Ross, *J. Electrochem. Soc.* **2001**, *148*, A1341.
[39] H. Wang, D. Yu, C. Kuang, L. Cheng, W. Li, X. Feng, Z. Zhang, X. Zhang, Y. Zhang, *Chem* **2019**, *5*, 313.
[40] A. Wang, S. Kadam, H. Li, S. Shi, Y. Qi, *npj Comput. Mater.* **2018**, *4*, 1.
[41] B. Philippe, M. Valvo, F. Lindgren, H. Rensmo, K. Edström, *Chem. Mater.* **2014**, *26*, 5028.
[42] S. E. Sloop, J. K. Pugh, S. Wang, J. Kerr, K. Kinoshita, *Electrochem. Solid-State Lett.* **2001**, *4*, A42.
[43] E. Markevich, R. Sharabi, H. Gottlieb, V. Borgel, K. Fridman, G. Salitra, D. Aurbach, G. Semrau, M. Schmidt, N. Schall, C. Bruenig, *Electrochem. Commun.* **2012**, *15*, 22.
[44] V. K. C. Chau, Z. Chen, H. Hu, K.-Y. Chan, *J. Electrochem. Soc.* **2016**, *164*, A284.
[45] D. Aurbach, B. Markovsky, A. Rodkin, E. Levi, Y. Cohen, H.-J. Kim, M. Schmidt, *Electrochim. Acta* **2002**, *47*, 4291.
[46] S. Lux, I. Lucas, E. Pollak, S. Passerini, M. Winter, R. Kostecki, *Electrochem. Commun.* **2012**, *14*, 47.
[47] S.-Y. Li, P.-H. Ma, X.-L. Cui, Q.-D. Ren, F.-Q. Li, *J. Chem. Sci.* **2008**, *120*, 289.
[48] D. Aurbach, A. Zaban, Y. Gofer, Y. E. Ely, I. Weissman, O. Chusid, O. Abramson, *J. Power Sources* **1995**, *54*, 76, proceedings of the Seventh International Meeting on Lithium Batteries.
[49] B.-H. Zhu, C.-Z. Ni, N.-N. Wang, X.-Y. Zhao, W.-Q. Guo, P.-M. Zhang, J.-J. Zhang, S.-Q. Chen, W.-D. Lv, Y. Zhu, *Chin. Chem. Lett.* **2016**, *27*, 864.
[50] H. Wu, H. Jia, C. Wang, J.-G. Zhang, W. Xu, *Adv. Energy Mater.* **2021**, *11*, 2003092.
[51] J. Young, P. M. Kulick, T. R. Juran, M. Smeu, *ACS Appl. Energ. Mater.* **2019**, *2*, 1676.
[52] H. Kumar, E. Detsi, D. P. Abraham, V. B. Shenoy, *Chem. Mater.* **2016**, *28*, 8930.
[53] K. Leung, *Chem. Phys. Lett.* **2013**, *568*, 1.
[54] C. Peschel, F. Horsthemke, M. Leißing, S. Wiemers-Meyer, J. Henschel, M. Winter, S. Nowak, *Batteries & Supercaps* **2020**, *3*, 1183.
[55] G. V. Zhuang, K. Xu, H. Yang, T. R. Jow, P. N. Ross, *J. Phys. Chem. B* **2005**, *109*, 17567.
[56] M. Onuki, S. Kinoshita, Y. Sakata, M. Yanagidate, Y. Otake, M. Ue, M. Deguchi, *J. Electrochem. Soc.* **2008**, *155*, A794.
[57] Y. Lee, J. Lee, H. Kim, K. Kang, N.-S. Choi, *J. Power Sources* **2016**, *320*, 49.
[58] L. Fan, S. Chen, R. Ma, J. Wang, L. Wang, Q. Zhang, E. Zhang, Z. Liu, B. Lu, *Small* **2018**, *14*, 1801806.
[59] T. Stuyver, F. De Proft, P. Geerlings, S. Shaik, *J. Am. Chem. Soc.* **2020**, *142*, 10102.
[60] R. Pal, P. K. Chattaraj, *J. Comput. Chem.* **2023**, *44*, 278 .
[61] R. G. Pearson, *J. Mol. Struct.* **1992**, *255*, 261.
[62] K. Ushirogata, K. Sodeyama, Y. Okuno, Y. Tateyama, *J. Am. Chem. Soc.* **2013**, *135*, 11967.
[63] M. Shakourian-Fard, G. Kamath, S. M. Taimoory, J. F. Trant, *J. Phys. Chem. C* **2019**, *123*, 15885.
[64] R. G. Pearson, *Inorg. Chem.* **1988**, *27*, 734.
[65] R. Parr and W. Yang (1989), *Density-Functional Theory of Atoms and Molecules*, Oxford University Press, New York, Oxford .
[66] F. Ren, W. Zuo, X. Yang, M. Lin, L. Xu, W. Zhao, S. Zheng, Y. Yang, *J. Phys. Chem. C* **2019**, *123*, 5871.
[67] J. Yang, Q. Liu, K. Z. Pupek, T. L. Dzwiniel, N. L. Dietz Rago, J. Cao, N. Dandu, L. Curtiss, K. Liu, C. Liao, Z. Zhang, *ACS Energy Lett.* **2021**, *6*, 371.
[68] Y. Sasaki, M. Takehara, S. Watanabe, M. Oshima, N. Nanbu, M. Ue, *Solid State Ionics* **2006**, *177*, 299.
[69] V. García-Melgarejo, J. Alejandre, E. Núñez-Rojas, *J. Phys. Chem. B* **2020**, *124*, 4741.
[70] T. D. Pham, K.-K. Lee, *Small* **2021**, *17*, 2100133.

[71] B. S. Parimalam, B. L. Lucht, *J. Electrochem. Soc.* **2018**, *165*, A251.
[72] G. G. Eshetu, T. Diemant, M. Hekmatfar, S. Grugeon, R. J. Behm, S. Laruelle, M. Armand, S. Passerini, *Nano Energy* **2019**, *55*, 327.
[73] M. P. Do, N. Bucher, A. Nagasubramanian, I. Markovits, T. Bingbing, P. J. Fischer, K. P. Loh, F. E. Kühn, M. Srinivasan, *ACS Appl. Mater. Interfaces* **2019**, *11*, 23972, pMID: 31251014.
[74] L. Lutz, D. Alves Dalla Corte, M. Tang, E. Salager, M. Deschamps, A. Grimaud, L. Johnson, P. G. Bruce, J.-M. Tarascon, *Chem. Mater.* **2017**, *29*, 6066.
[75] M. Nie, B. L. Lucht, *J. Electrochem. Soc.* **2014**, *161*, A1001.
[76] M. Zhou, P. Bai, X. Ji, J. Yang, C. Wang, Y. Xu, *Adv. Mater.* **2021**, *33*, 2003741.
[77] M. Ue, *J. Electrochem. Soc.* **1994**, *141*, 3336.
[78] V. Aravindan, J. Gnanaraj, S. Madhavi, H.-K. Liu, *Chem. Eur. J.* **2011**, *17*, 14326.
[79] M. Murakami, H. Yamashige, H. Arai, Y. Uchimoto, Z. Ogumi, *Electrochem. Solid-State Lett.* **2011**, *14*, A134.
[80] T. Thomberg, R. Väli, J. Eskusson, T. Romann, A. Jänes, *J. Electrochem. Soc.* **2018**, *165*, A3862.
[81] M. Ue, S. Mori, *J. Electrochem. Soc.* **1995**, *142*, 2577.
[82] T. Hosaka, K. Kubota, H. Kojima, S. Komaba, *Chem. Commun.* **2018**, *54*, 8387.
[83] K. Yoshida, M. Nakamura, Y. Kazue, N. Tachikawa, S. Tsuzuki, S. Seki, K. Dokko, M. Watanabe, *J. Am. Chem. Soc.* **2011**, *133*, 13121.
[84] D. M. Seo, S. Reininger, M. Kutcher, K. Redmond, W. B. Euler, B. L. Lucht, *J. Phys. Chem. C* **2015**, *119*, 14038.
[85] C. Sheng, F. Yu, C. Li, H. Zhang, J. Huang, Y. Wu, M. Armand, Y. Chen, *J. Phys. Chem. Lett.* **2021**, *12*, 2064.
[86] Gaussian 16, Revision C.01, M. J. Frisch, et al., Gaussian, Inc., Wallingford CT, **2019** (Please see SI for full citation).
[87] Y. Zhao, D. G. Truhlar, *Theor. Chem. Acc.* **2008**, *120*, 215.
[88] X. Li, M. J. Frisch, *J. Chem. Theory Comput.* **2006**, *2*, 835.
[89] A. V. Marenich, C. J. Cramer, D. G. Truhlar, *J. Phys. Chem. B* **2009**, *113*, 6378.

Manuscript received: September 28, 2022
Revised manuscript received: December 11, 2022
Accepted manuscript online: December 21, 2022
Version of record online: January 23, 2023